Research Article Vol. 34, No. 10 / 18 May 2026 / Optics Express 18037
Optics EXPRESS

Optimized weak fiber Bragg array interrogation system based on adaptive gain and polynomial fitting method

CAILING FU,[1,2] HUAFENG ZHA,[1,2] PING CHEN,[1,2] YABO SHI,[1,2] NIANQING ZOU,[1,2] RONGYI SHAN,[1,2] SHIJIE LI,[1,2] HUAJIAN ZHONG,[1,2] YONGZHENG XU,[1,2] WEIJIA BAO,[1,2] AND YIPING WANG[1,2,*]

[1]*State Key Laboratory of Radio Frequency Heterogeneous Integration, Key Laboratory of Optoelectronic Devices and Systems of Ministry of Education/Guangdong Province, College of Physics and Optoelectronic Engineering, Shenzhen University, Shenzhen 518060, China*
[2]*Shenzhen Key Laboratory of Photonic Devices and Sensing Systems for Internet of Things, Guangdong and Hong Kong Joint Research Centre for Optical Fibre Sensors, Shenzhen University, Shenzhen 518060, China*
[*]*ypwang@szu.edu.cn*

Abstract: An optimized WFBGA interrogation system based on an adaptive gain control and polynomial fitting algorithm is demonstrated, achieving the demodulation of WFBGA containing 1000 WFBGs with a reflectivity of -40 dB and a spacing of 1.5 m. To avoid the trade-off between the saturation of frontend WFBGs and the low amplitude of backend WFBGs in the fixed gain, an adaptive gain control method is adopted to maintain the reflection amplitude of each WFBG at the preset threshold, i.e., -35 and -34 dBm, by independently and dynamically adjusting the driving current of each WFBG through address scanning. Compared with the centroid and Gaussian fitting methods, the polynomial method exhibited superior stability, i.e., minimal wavelength fluctuation, and excellent consistency, i.e., minimal wavelength error.

1. Introduction

Weak fiber Bragg grating arrays (WFBGAs) have been widely used in the fields of aerospace structural health monitoring [1], bridges [2] and tunnels safety monitoring [3], oil and gas pipeline leakage detection [4] for measuring temperature, strain and vibration distribution, due to its quasi-distributed sensing capability and high reliability. To achieve wavelength demodulation of WFBGA, various demodulation schemes have been developed, including frequency domain reflectometry (OFDR) based on the frequency domain and optical time domain reflectometry (OTDR) based on the time domain [5]. For example, OFDR was employed to achieve the demodulation of large-scale multiplexing of 10000 FBGs along a 10 m long fiber, where the length and spacing of WFBG was randomly varied around 0.5 mm and 1.5 mm, respectively [6]. However, long-distance demodulation of WFBGAs remains difficult because of the nonlinear error accumulation of the tunable laser source (TLS) and the attenuation of backscattering signals. Currently, the demodulation methods for WFBGAs based on OTDR are mainly divided into wavelength scanning based on TLS and photodetector [7], and pulse phase-shift based on amplified spontaneous emission (ASE) and charge-coupled device (CCD) [8]. Han *et al.* used a narrow bandwidth filter to translate wavelength shift to intensity measurement, and achieved high-speed demodulation of 342 WFBGs along an 855 m long fiber [9]. A spatial resolution of 0.16 m with an interrogation error of 13.98 pm was realized over a 250-286 m sensing array using double wide pulse signals based on TLS [10]. Two semiconductor optical amplifiers (SOAs) were incorporated to regulate the time delay, enabling the interrogation of 843 WFBGs with a spatial resolution of 2 m [11]. Moreover, a field-programmable gate array (FPGA)-based large-capacity

#592728 https://doi.org/10.1364/OE.592728
Journal © 2026 Received 4 Feb 2026; revised 17 Apr 2026; accepted 21 Apr 2026; published 7 May 2026

Optics EXPRESS

sensing network was constructed to interrogate 1642 serial time-division-multiplexing WFBGs with a peak reflectivity of −40 dB and equal separations of 2.5 m [12]. However, as the number of WFBG increased and the sensing distance extends, the reflected signals from WFBGs located at the array's end or with lower reflectivity were significantly attenuated due to transmission loss and the cumulative effect of multiple reflections [13].

In this paper, an optimized interrogation system for WFBGA is proposed based on an adaptive gain approach combined with a polynomial fitting algorithm, achieving the demodulation of 1000 WFBGs with a reflectivity of -40 dB and a spacing of 1.5 m. In the adaptive method, the reflection amplitude of each WFBG is monitored in real-time, and the gain of the EDFA is dynamically adjusted to adaptively match the gain for different WFBGs, which ensured sufficient amplification of the WFBG at the backend and effectively prevented over-amplification of the WFBGs at the frontend. The experimental setup and workflow of the optimized WFBGA interrogation system are firstly introduced. Then the detailed process of the address scanning and adaptive gain in FPGA are studied. Moreover, the reflection spectra of WFBGA under fixed gain and adaptive gain are investigated and compared. Furthermore, the wavelength fluctuation and errors of three fitting algorithms, i.e., centroid, gaussian, and polynomial, are compared. Finally, the effects of adaptive gain adjustment on the Bragg wavelength and spectral profile under different driving currents are analyzed.

2. Experimental setup and principle

As shown in Fig. 1, an optimized weak fiber Bragg grating array (WFBGA) interrogation system based on adaptive gain control of erbium-doped fiber amplifier (EDFA) was established [14]. The system consisted of three parts: the optical devices, FPGA-implemented delay control and data acquisition, and polynomial fitting-based demodulation. The light emitted from the amplified spontaneous emission (ASE) was transmitted through the isolator and was then launched into the first semiconductor optical amplifier (SOA), i.e., SOA1, where it was modulated into narrow optical pulses with a pulse width of t_0 and period of T, driven by the pulse generator in the FPGA. Then, the modulated pulses were amplified by EDFA and injected into the WFBGA through the circulator. Note that the WFBGA was fabricated using the femtosecond laser point-by-point technology [15], with a reflectivity of -40 dB, a grating spacing of 1.5 m, and a total of 1000 WFBGs, i.e., R = -40 dB, d = 1.5 m, N = 1000, respectively. Subsequently, the pulses reflected back from the WFBGA were output to SOA2 through another port of the circulator. Here, the time delay of the reflected pulses of $\mathrm{WFBG_i}$ reaching SOA2, i.e., τ_i, was given by [16]

$$\tau_i = \frac{2n[l_0 + d(i-1)]}{c} \tag{1}$$

where n is the effective refractive index, l_0 is the distance between $\mathrm{WFBG_1}$ and the circulator, and d is the grating spacing of the WFBG, c is the speed of light in vacuum. Thus, the reflected pulses of each WFBG in WFBGA reach SOA2 in sequence based on Eq. (1).

To capture the reflected pulses from individual WFBGs, the pulse delay implemented in the FPGA was used to control the time-domain gating of SOA2. The time shift between the driving pulse of SOA2 and SOA1 was set to τ_i, corresponding to the arrival time delay of the $\mathrm{WFBG_i}$ reflected pulse, as shown in Fig. 2. By controlling the delay of SOA2 to τ_1, τ_2, τ_3, . . . , τ_n, the reflected pulses of $\mathrm{WFBG_1}$, $\mathrm{WFBG_2}$, $\mathrm{WFBG_3}$, . . . , $\mathrm{WFBG_n}$ were selectively captured. And the strict sequential timing constraints of SOA1 and SOA2 were imposed by pulse generator and pulse delay, respectively. When the reflected pulse of $\mathrm{WFBG_i}$ was selected, the CCD line was synchronously driven by CCD control in FPGA to complete photoelectric conversion via clock (CLK) and exposure time (ET) signals. Note that the ET was longer than the pulse width of SOA2. To avoid spectral truncation or energy loss, the timing constraint required that reflected pulses were fully confined within the exposure window of the CCD, as shown in Fig. 2. Driven by

Optics EXPRESS

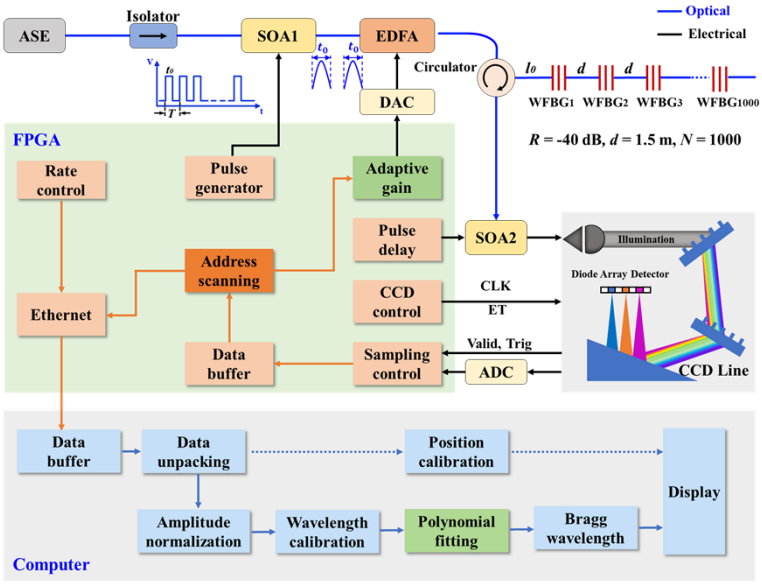

Fig. 1. Schematic diagram of optimized weak fiber Bragg array (WFBGA) interrogation system based on adaptive gain of erbium-doped fiber amplifier (EDFA), consisting of three parts: optical devices, a field programmable gate array (FPGA)- implemented delay control and data acquisition, as well as a polynomial fitting-based demodulation. ASE: amplified spontaneous emission; SOA: semiconductor optical amplifier; DAC: digital-to-analog converter; ADC: analog to digital converter; CLK: clock; ET: exposure time. Note that the WFBGA was fabricated using the femtosecond laser point-by-point technology, with the reflectivity, spacing, and number of the WFBG being -40 dB, 1.5 m, and 1000, i.e., R = -40 dB, d = 1.5 m, N = 1000, respectively.

the ET signal, the complete photoelectric conversion was performed to output an analog spectral signal, i.e., 256 pixels in sequence, after 8 CLK cycles. A valid signal was simultaneously fed back to the FPGA, marking the completion of the conversion process. In addition, a trigger signal was also synchronously generated by CCD for initiating analog-to-digital conversion (ADC). When the valid signal was pulled high, the spectral acquisition of WFBG was initiated. Note that the sampling clock and trigger signal should be completely synchronized, as shown in Fig. 2. At this time, the spectral acquisition of WFBG was completed.

Subsequently, the acquired spectrum, i.e., 256 pixels, through ADC were cached, i.e., data buffer, and sent to address scanning for calibrating the delay of WFBG. Based on the obtained amplitude of WFBG, the gain coefficient of EDFA is adaptively adjusted by driving a digital-to-analog converter (DAC) to convert digital into analog gain. Then the spectrum and corresponding delay were packaged and transmitted to the computer through the ethernet, and then unpackaged. Note that the transmission rate was scheduled by rate controller to match the demodulation rate. Here, the delay was employed to calibrate the position of each WFBG. And the spectrum was subjected to amplitude normalization and wavelength calibration. Then three fitting algorithms, including centroid, Gaussian, and polynomial, were used to extract the Bragg wavelength of each WFBG. Finally, the demodulated Bragg wavelengths of WFBGs are mapped to their corresponding positions and displayed in real time.

The detailed process of the address scanning and adaptive gain in FPGA is shown in Fig. 3(a). Firstly, sampling was performed to obtain the time-domain signal of the WFBGA. Taking $WFBG_1$ as an example, when the reflected pulses passed through SOA2 and moved from left to right with a step of 1 ns, it entered the gating window in a partially covered, fully covered, or partially covered

Optics EXPRESS

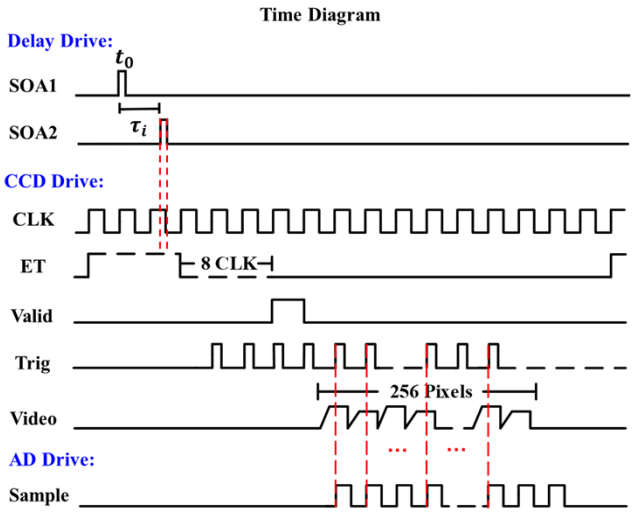

Fig. 2. Timing of delay drive, CCD drive, and AD drive for the optimized WFBGA interrogation system. Note t_0 is the pulse width modulated by SOA1, τ_i is the delay of the reflected pulses of $WFBG_i$ reaching SOA2.

state in sequence, as shown in Fig. 3(b). Note that SOA2 was equivalent to an optical switch with a gating window of 6 ns to ensure reliable time-domain separation of two adjacent reflected signals of WFBGs. Then the entire duration from its entry to complete departure generated an effective acquisition interval of approximately 12 ns, corresponding to the amplitudes of a_1, a_2, a_3, . . . , and a_{11}. Obviously, the amplitude was first increased and then decreased. Secondly, the amplitude threshold was set to -40 dBm, i.e., TH = -40 dBm, to suppress the noise. And the maximum amplitude in each WFBG scanning sequence was identified, i.e., peak detection, to obtain the corresponding delay of each WFBG. The maximum amplitudes of $WFBG_1$, $WFBG_2$, and $WFBG_3$ were a_6, b_6, c_6, i.e., the pulse fully fell within the gating window, as shown in Fig. 3(c), corresponding to the delays of 12, 23, 34 ns, respectively. In this way, the delay of each WFBG could be obtained and stored in block random access memory (BRAM1). Then the delay was sequentially read by the read controller, i.e., RD CTRL, and sent to the delay control to achieve delay control of SOA2. In this way, the address scanning of each WFBG could be achieved by controlling the delay of SOA1 and SOA2. Subsequently, an adaptive gain was introduced to dynamically adjust the reflection amplitude of each WFBG. Taking $WFBG_i$ as an example, the obtained reflection amplitude was compared with the set threshold to determine if the amplitude difference between the two was within the range. If it is within the range, the current gain coefficient was stored in BRAM2 and the read address was increased by 1, i.e., performing address scanning on $WFBG_{i+1}$. If not, the gain adjustment was performed. When the amplitude was below the threshold, the EDFA gain was increased; otherwise, decreased it. Note that the adaptive gain was adjusted using a fixed current step of 2 mA. The adjusted digital gain was converted to analog by DAC and applied to EDFA through current control. Repeating the above steps until the reflection amplitude of corresponding WFBG was within the range. In addition, the total time consumption for each WFBG was about 80 µs, including 60 µs for CCD spectral acquisition and 20 µs for signal processing. The gain adjustment time of the EDFA was about 20 µs, which is shorter than the time required for signal acquisition and processing of each WFBG. Therefore, the EDFA gain adjustment is completed before scanning the next WFBG, introducing no additional time overhead. In this way, the delay and gain coefficients

Optics EXPRESS

stored in BRAM1 and BRAM2 were read separately to control SOA2 delay and EDFA gain, thereby stabilizing the reflection amplitude of each WFBG at the preset threshold.

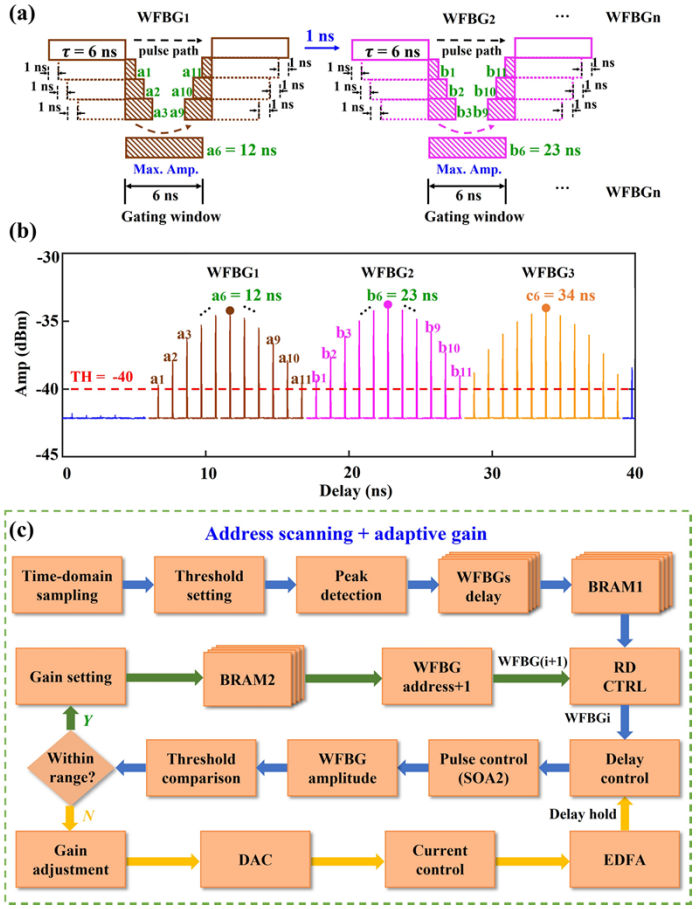

Fig. 3. (a) Detailed flowchart of address scanning and adaptive gain in FPGA; (b) Schematic diagram of the time-domain scanning path of WFBG's reflected pulses passing through SOA2, i.e., an optical switch with a gating window of 6 ns, in a partially covered, fully covered, or partially covered state in sequence; (c) time-domain signal of $WFBG_1$, $WFBG_2$, and $WFBG_3$, corresponding to the delays of 12, 23, and 34 ns, respectively. BRAM: block random access memory; RD CTRL: read control; TH: threshold.

3. Experimental results and discussions

To verify the performance of the proposed adaptive gain method, the reflection spectra of WFBGA under fixed gain and adaptive gain was investigated and compared. Under a fixed gain with a driving current of 130 mA i.e., $I = 130$ mA, the amplitude exhibited an attenuation from -34 to -42 dBm, as illustrated in Fig. 4(a). Specifically, the amplitudes of the first 15 WFBGs, i.e., $WFBG_1$ to $WFBG_{15}$, were effective compensated and remained at approximately -34 dBm, with their reflection spectra presenting a regular profile, as shown in Fig. 4(b). In contrast, the amplitudes of the backends WFBGs, i.e., $WFBG_{986}$ to $WFBG_{1000}$, gradually deteriorated to the noise floor, making it difficult for the CCD to detect the signal, as shown in Fig. 4(c). Note that the detection range of the CCD was from -44 to -30 dBm. Subsequently, the driving current was increased to 150 mA, i.e., $I = 150$ mA, to detect the WFBG signal at the backend. As shown in Fig. 4(d),

Optics EXPRESS

the amplitude was attenuated from -30 to -40 dBm. Obviously, the amplitudes of the backend WFBGs, i.e., $WFBG_{986}$ to $WFBG_{1000}$, were compensated to approximately -40 dBm, with a regular reflection spectral profile, as illustrated in Fig. 4(f). However, the reflection peaks of the frontend WFBGs, i.e., $WFBG_1$ to $WFBG_{15}$, were distorted due to CCD operating in the nonlinear saturation region, exhibiting spectral flattening and broadening, as illustrated in Fig. 4(e). The phenomenon indicated that the frontend WFBGs were excessively amplified under a driving current of 150 mA, while the backend WFBGs were not effectively compensated under a driving current of 130 mA. Therefore, the trade-off between saturation of the frontend WFBGs and low amplitude of the backend WFBGs proved irreconcilable under a fixed gain. In the adaptive gain mode, the driving current for each WFBG was independently adjusted via address scanning, enabling the amplitude of the WFBGA to be stably maintained at the preset threshold of -35 dBm without any attenuation, as illustrated in Fig. 4(g). Note that the preset threshold was set to -35 dBm to avoid both the noise floor and the saturation region. Moreover, the amplitudes of the frontend and backend WFBGs were comparable with regular spectral profiles, as shown in Figs. 4(h) and 4(i).

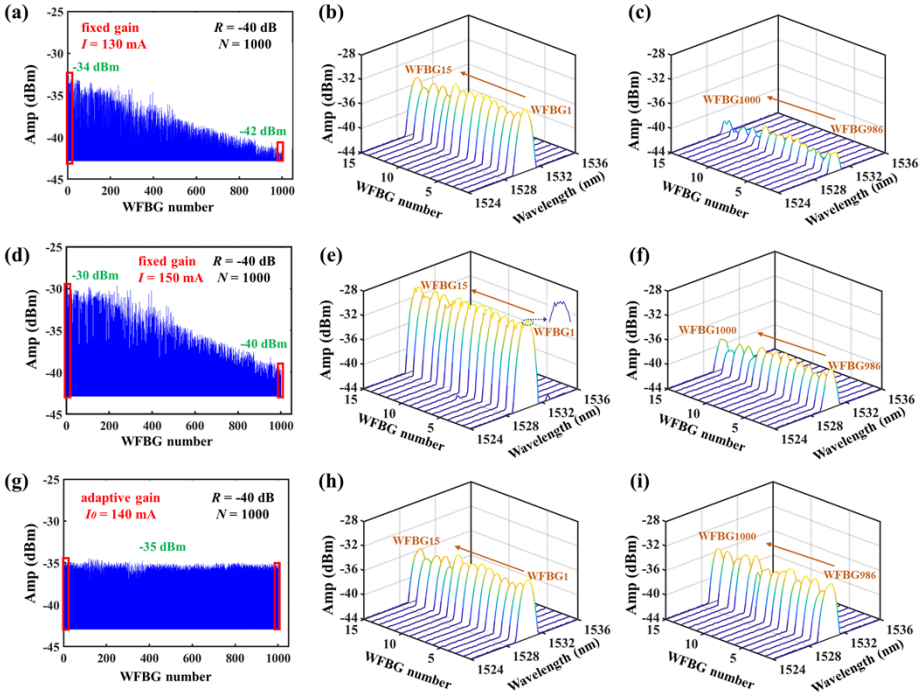

Fig. 4. Demodulated reflection amplitude of the WFBGA, reflection spectra of the first 15 WFBGs, i.e., $WFBG_1$ to $WFBG_{15}$, and the last 15 WFBGs, i.e., $WFBG_{986}$–$WFBG_{1000}$ under different operating modes: (a, d, g) WFBGA demodulated reflection amplitude; (b, e, h) first 15 WFBGs; (c, f, i) last 15 WFBGs. Operating modes: (a–c) fixed gain mode with a driving current of 130 mA; (d–f) fixed gain mode with a driving current of 150 mA; (g–i) adaptive gain mode with a preset threshold of −35 dBm. Note that the reflectivity and the number of WFBG were -40 dB and 1000, i.e., R = -40 dB, N = 1000, and the initial gain current was 140 mA, i.e., I_0=140 mA, respectively.

Compared to the amplitude attenuation in the fixed gain mode, the amplitude in the adaptive gain mode was remained at the preset threshold of -35 dBm under the initial driving current of 150 and 130 mA, as shown in Fig. 5(a). Compared to the 150 mA driving current in the fixed gain mode, the driving current of the frontend WFBGs with smaller attenuation was adaptively

Optics EXPRESS

adjusted to below 150 mA, while that of the backend WFBGs with larger attenuation was adjusted to above 150 mA, as shown in Fig. 5(b). Overall, the driving current was increased from 114 mA to 174 mA as the WFBG number rose to 1000. Similarly, the trend of adaptive adjustment process under initial driving current of 130 mA was the same as that under 150 mA, as illustrated in Fig. 5(c). Subsequently, the preset threshold of amplitude was increased to -34 dBm. As shown in Fig. 5(d), the amplitude of the WFBGA was stably maintained at -34 dBm at initial driving currents of 150 and 130 mA. And the driving current was adaptively reduced for the frontend WFBGs with high reflection amplitudes, while it was increased for the backend WFBGs with low reflection amplitudes, as shown in Figs. 5(e) and 5(f). This indicated that the proposed adaptive gain method could achieve stable and uniform gain adjustment to the preset threshold amplitude based on the actual reflected amplitude of each WFBG, regardless of the initial gain current.

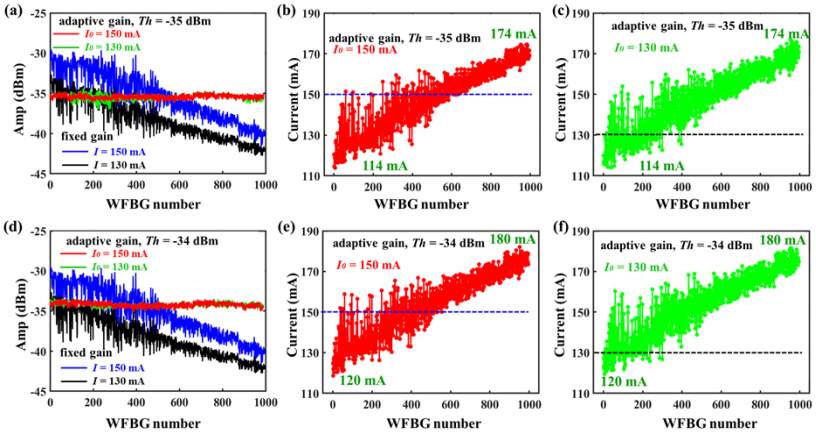

Fig. 5. (a) Demodulated reflection amplitude of WFBGA in two gain modes: fixed gain with driving currents of 150 mA and 130 mA, and adaptive gain (preset threshold of -35 dBm) with initial driving currents of 150 mA and 130 mA; driving currents of individual WFBGs under initial driving currents of (b) 150 mA and (c) 130 mA, respectively; (d) demodulated reflection amplitude of WFBGA in two gain modes: fixed gain with driving currents of 150 mA and 130 mA, and adaptive gain (preset threshold of -34 dBm) with initial driving currents of 150 mA and 130 mA; driving currents of individual WFBGs under initial driving currents of (b) 150 mA and (c) 130 mA.

To achieve demodulation of the Bragg wavelengths for the WFBGA, the performance of four fitting algorithms, i.e., centroid fitting, gaussian fitting, polynomial fitting, and wavelet-transform-assisted polynomial fitting, was systematically compared and evaluated using 1000 consecutive measurements. Specifically, the Bragg wavelengths of $WFBG_{300}$, $WFBG_{600}$, $WFBG_{900}$, and $WFBG_{1000}$ were subjected to fitting and performance comparison. As shown by the blue curve in Fig. 6, the wavelength fluctuation s, i.e., the difference between the maximum and minimum fitted Bragg wavelengths, of WFB_{300}, $WFBG_{600}$, $WFBG_{900}$, and $WFBG_{1000}$ using the centroid fitting were 38 pm, 35 pm, 35 pm, and 39 pm, respectively. When gaussian fitting was adopted, the corresponding Bragg wavelength fluctuation s were significantly reduced to 18 pm, 19 pm, 18 pm and 22 pm, respectively, as shown by the red curve in Fig. 6. Compared with the centroid fitting and gaussian fitting methods, polynomial fitting exhibited the minimal wavelength fluctuation s of 8 pm, 7 pm, 9 pm, and 10 pm, respectively. Note that the 2^{nd}-order polynomial fitting was used in the experiment. Moreover, wavelet-transform-assisted polynomial fitting yielded the smallest wavelength fluctuations of 4 pm, 3 pm, 3 pm, and 4 pm, respectively. This indicated that wavelet-transform preprocessing can effectively suppress random noise and further enhance the peak-tracking performance of polynomial fitting.

Optics EXPRESS

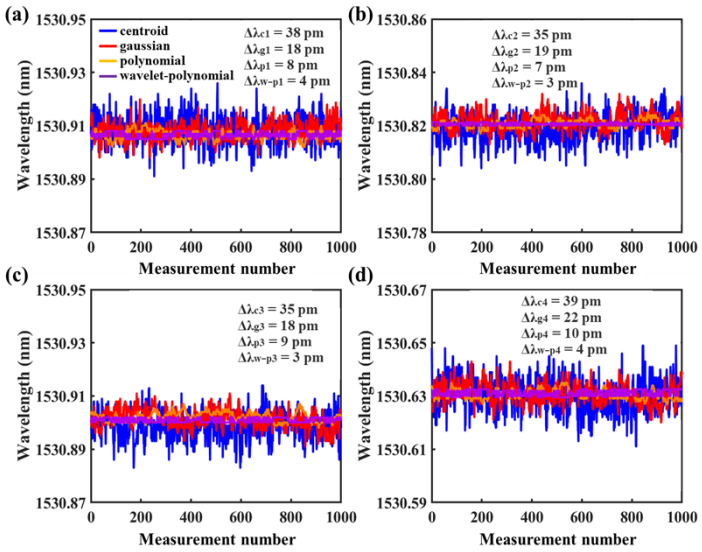

Fig. 6. Bragg wavelength fluctuations of (a) $WFBG_{300}$, (b) $WFBG_{600}$, (c) $WFBG_{900}$, and (d) $WFBG_{1000}$ obtained via centroid, Gaussian, polynomial and wavelet-transform-assisted polynomial fitting algorithms under 1000 consecutive measurements.

Moreover, the wavelength errors for $WFBG_{300}$, $WFBG_{600}$, and $WFBG_{900}$ was further investigated and compared under four algorithms. As shown in Fig. 7(a), the initial bragg wavelength of $WFBG_{300}$ was at 1530.909 nm. By contrast, the Bragg wavelengths derived from the centroid, gaussian, polynomial, and wavelet-transform-assisted polynomial fitting were 1530.921, 1530.915, 1530.914, and 1530.910 nm, corresponding to wavelength errors of 12 pm, 6 pm, 5 pm, and 1 pm, respectively. For $WFBG_{600}$, the corresponding errors were 15 pm, 2 pm, 5 pm, and 4 pm, respectively, as illustrated in Fig. 7(b); For $WFBG_{900}$, the corresponding errors were 26 pm, 16 pm, 4 pm, and 4 pm, respectively, as shown in Fig. 7(c). Obviously, centroid fitting exhibited the largest wavelength errors among four algorithms, with the deviations being significantly higher than those of Gaussian and polynomial fitting. When the spectral profile of $WFBG_{600}$ conformed to a Gaussian distribution, the wavelength error was minimized at 2 pm, i.e., $\Delta\lambda_{g2'}$=2 pm. In contrast, when the spectral profile exhibited asymmetric distortion, i.e., $WFBG_{900}$, the wavelength error increased significantly to 16 pm, i.e., $\Delta\lambda_{g2'}$=16 pm. This indicated that Gaussian fitting was highly sensitive to spectral profile mismatch, and its demodulation stability was significantly affected by the spectral profile. Compared with centroid and Gaussian fitting methods, wavelet-transform-assisted polynomial fitting method exhibited good consistency with wavelength errors of 1 pm, 4 pm, and 4 pm for $WFBG_{300}$, $WFBG_{600}$, and $WFBG_{900}$, respectively. However, the wavelet preprocessing significantly increases the computational cost and algorithmic complexity in WFBGA demodulation. Therefore, the polynomial fitting method was ultimately adopted to demodulate the WFBG based on the minimum wavelength fluctuation and wavelength error discussed above.

To verify the effect of adaptive gain adjustment on the demodulation, the Bragg wavelength and spectral profile under different EDFA driving currents were studied. As shown in Fig. 8(a), when the driving current was increased from 110 to 140 mA, the Bragg wavelengths of $WFBG_{200}$ in the raw spectrum were fixed at 1530.258 nm. And the Bragg wavelengths of $WFBG_{500}$ and $WFBG_{800}$ were at 1530.053, and 1530.738 nm, corresponding to the driving currents of 130 to 160 mA, and 150 to 180 mA, respectively. And the amplitude was increased with the increase of driving current. As shown in Fig. 8(b), the overall profile of all spectra exhibited good consistency

Optics EXPRESS

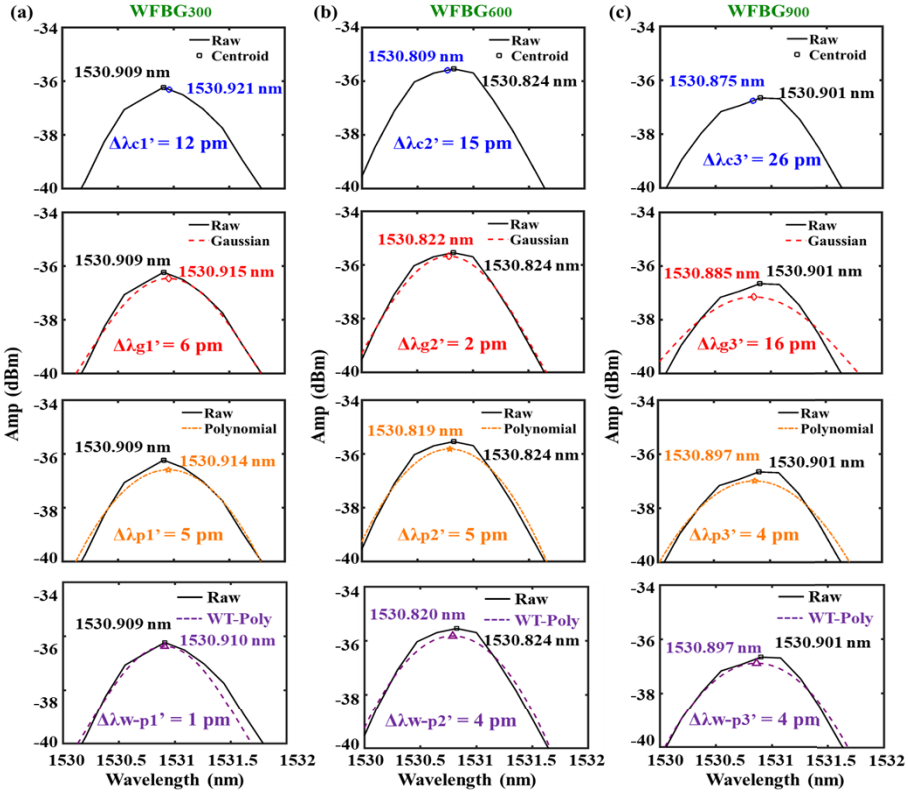

Fig. 7. Reflection spectra of (a) $WFBG_{300}$, (b) $WFBG_{600}$, and (c) $WFBG_{900}$ fitted using centroid, gaussian, polynomial, and wavelet-transform-assisted polynomial fitting algorithms.

without abnormal features such as spectral broadening, peak shape deviation or distortion. Under driving currents of 110, 120, 130, 140 mA, the Bragg wavelengths of $WFBG_{200}$ fitted with polynomial algorithms were 1530.263, 1530.253, 1530.262, 1530.260 nm, respectively. And the maximum deviation of the fitted wavelength from the initial wavelength was 5 pm for $WFBG_{200}$. As with the $WFBG_{200}$, the effect of the driving current on the $WFBG_{500}$ and $WFBG_{800}$ was only reflected in the fluctuation of amplitude. Moreover, the maximum deviation of the fitted wavelength was 6 pm and 7 pm for $WFBG_{500}$ and $WFBG_{800}$. Obviously, the maximum deviation points of the three WFBGs occurred at driving currents of 110, 130, and 150 mA, respectively, which can be mainly attributed to the lowest peak amplitude and the flattening of the spectral tops under these conditions. This feature reduced the accuracy of peak fitting and then exacerbate the wavelength error. Thus, the consistency and stability of the demodulated Bragg wavelength could be guaranteed during the adaptive gain process. To further verify the sensing performance of the optimized WFBGA interrogation system based on adaptive gain and polynomial fitting, the strain sensing property of WFBGA was investigated. When the strain was increased from 0 to 8000 με with a step of 500 με, the Bragg wavelengths of $WFBG_{10}$ and $WFBG_{990}$ both exhibited a linear redshift, with corresponding linear coefficient of 99.96% and 99.90%, as illustrated in Figs. 8(a) and 8(b). Moreover, the strain sensitivity was 1.1 pm/με, which consistent with the strain sensitivity of SMF [17]. In addition, the residuals of the linear fitting for both $WFBG_{10}$ and $WFBG_{990}$ were distributed around zero without obvious systematic deviation. The maximum absolute residuals were 0.056 nm and 0.011 nm, respectively, indicating a good

Optics EXPRESS

agreement between the measured Bragg wavelength Figs. 9 and the fitted Bragg wavelength. These results further confirmed the good linear strain response and fitting reliability.

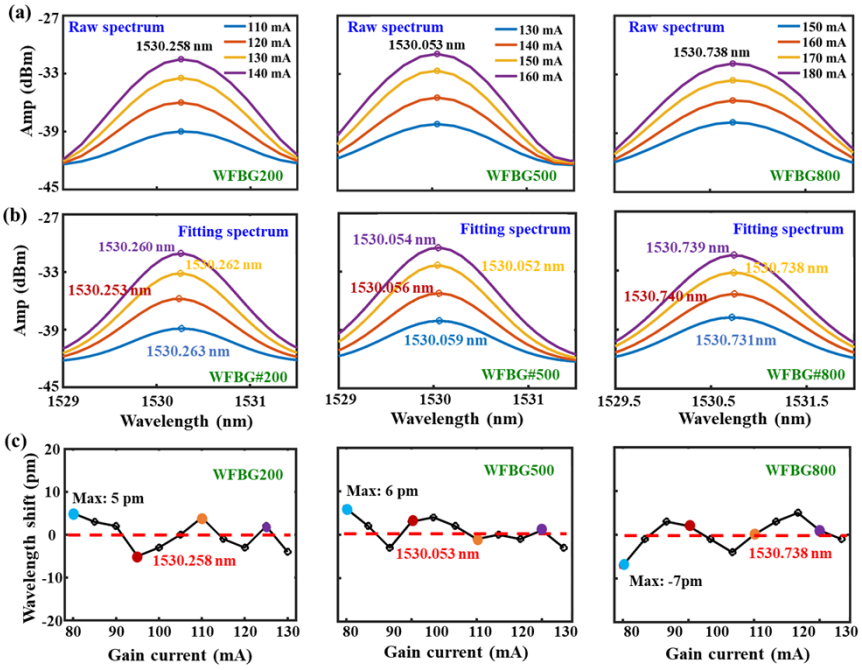

Fig. 8. Reflection spectra of $WFBG_{200}$, $WFBG_{500}$, and $WFBG_{800}$ obtained by (a) non-fitting, i.e., raw spectrum and (b) polynomial fitting; (c) wavelength shift between fitted and initial wavelength of $WFBG_{200}$, $WFBG_{500}$, and $WFBG_{800}$.

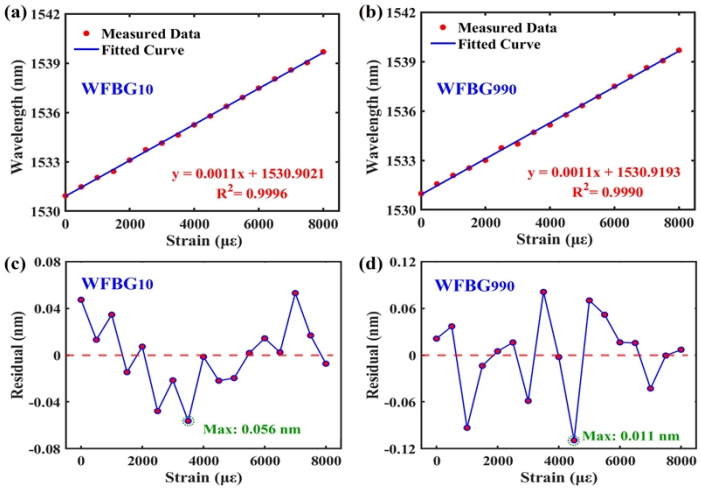

Fig. 9. Measured Bragg wavelength shifts of (a) $WFBG_{10}$ and (b) $WFBG_{990}$ as a function of the strain, together with the residuals of the corresponding linear fittings under different strain levels.

Optics EXPRESS

4. Conclusion

In conclusion, an optimized WFBGA interrogation system based on an adaptive gain control and polynomial fitting algorithm was demonstrated. A WFBGA containing 1000 WFBGs with a reflectivity of -40 dB and a spacing of 1.5 m was successfully demodulated. Under fixed gain, the trade-off between saturation of the frontend WFBGs and low amplitude of the backend WFBGs was irreconcilable. Under adaptive gain, the reflection amplitude of each WFBG was stably maintained at the preset threshold, i.e., -35 and -34 dBm, without attenuation by independently and dynamically adjusting the driving current of each WFBG through address scanning. Compared with the wavelength fluctuations of 38, 35, 35, and 39 pm for the centroid and 18, 19, 18, and 22 pm for the gaussian method, the polynomial method exhibits optimal stability with wavelength fluctuations of 8, 7, 9, and 10 pm for $WFBG_{300}$, $WFBG_{600}$, $WFBG_{900}$, and $WFBG_{1000}$, respectively. Moreover, the polynomial fitting method exhibited good consistency with wavelength errors of 5 pm, 5 pm, and 4 pm for $WFBG_{300}$, $WFBG_{600}$, and $WFBG_{900}$, respectively. And the consistency and stability of the demodulated Bragg wavelength can be guaranteed during the adaptive gain process.

Funding. National Key Research and Development Program of China (2023YFB3209500); National Natural Science Foundation of China (grant nos. U22A2088, 62375178, 62405196); Shenzhen Science and Technology Program (JCYJ20241202124226032); LingChuang Research Project of China National Nuclear Corporation (No. CNNC-LCKY-202265); China Postdoctoral Science Foundation (grant nos. 2024M752107).

Disclosures. The authors declare no conflicts of interest.

Data availability. Data underlying the results presented in this paper are not publicly available at this time but may be obtained from the authors upon reasonable request.

References

1. M. Liu, Y. Xu, J. Guo, *et al.*, "Multi-parameter information detection of aircraft taxiing on an airport runway based on an ultra-weak FBG sensing array," Opt. Express **32**(14), 25135–25146 (2024).
2. S. Li, J. Ma, W. Hu, *et al.*, "On-site experimental study on expressway disaster identification based on ultra-weak FBG sensor array," Dev. Built Environ **24**, 100777 (2025).
3. L. Xin, Z. Li, X. Gui, *et al.*, "Surface intrusion event identification for subway tunnels using ultra-weak FBG array based fiber sensing," Opt. Express **28**(5), 6794–6805 (2020).
4. T. Yang, Y. Xiao, Z. Ran, *et al.*, "Design of a weak fiber bragg grating acoustic sensing system for pipeline leakage monitoring in a nuclear environment," IEEE Sensors J. **21**(20), 22703–22711 (2021).
5. X. Gui, Z. Li, X. Fu, *et al.*, "Distributed optical fiber sensing and applications based on large-scale fiber bragg grating array: review," J. Lightwave Technol. **41**(13), 4187–4200 (2023).
6. X. Gui, Z. Li, X. Fu, *et al.*, "Large-scale multiplexing of a FBG array with randomly varied characteristic parameters for distributed sensing," Opt. Lett. **43**(21), 5259–5262 (2018).
7. K. Xu, F. Wang, Y. Wang, *et al.*, "Large-capacity interrogation for ultra-weak fiber bragg grating array with a DFB laser array chip," J. Lightwave Technol. **43**(17), 8467–8473 (2025).
8. C. Li, J. Tang, C. Cheng, *et al.*, "FBG arrays for quasi-distributed sensing: a review," Photon. Sens **11**(1), 91–108 (2021).
9. P. Han, Z. Li, L. Chen, *et al.*, "A high-speed distributed ultra-weak FBG sensing system with high resolution," IEEE Photon. Technol. Lett. **29**(15), 1249–1252 (2017).
10. J. Wang, Z. Li, X. Fu, *et al.*, "Interrogation of cascaded FBGs with narrow spacing using double wide pulse signals," IEEE Photon. Technol. Lett. **34**(21), 1175–1178 (2022).
11. C. Hu, H. Wen, W. Bai, *et al.*, "A novel interrogation system for large scale sensing network with identical ultra-weak fiber bragg gratings," J. Lightwave Technol. **32**(7), 1406–1411 (2014).
12. Z. Wang, H. Wen, C. Hu, *et al.*, "Field-programmable gate array-based large-capacity sensing network with 1642 ultra-weak fiber Bragg gratings," Chin. Opt. Lett. **14**(1), 010601 (2016).
13. W. Gao, J. Liu, H. Guo, *et al.*, "Multi-wavelength ultra-weak fiber bragg grating arrays for long-distance quasi-distributed sensing," Photon. Sens **12**(2), 185–195 (2022).
14. M. Yang, W. Bai, H. Guo, *et al.*, "Huge capacity fiber-optic sensing network based on ultra-weak draw tower gratings," Photon. Sens **6**(1), 26–41 (2016).
15. Z. Peng, Y. Shi, R. Sui, *et al.*, "Multi-channel OFDR strain sensor based on wavelength/space division multiplexing weak FBG arrays," J. Lightwave Technol. **43**(17), 8492–8497 (2025).
16. Z. Luo, H. Wen, H. Guo, *et al.*, "A time- and wavelength-division multiplexing sensor network with ultra-weak fiber bragg gratings," Opt. Express **21**(19), 22799–22807 (2013).
17. J. Yan, J. Zou, T. Xue, *et al.*, "Fiber bragg grating strain sensor with extended measurement range via strain relief ring," IEEE Sensors J. **25**(2), 2675–2681 (2025).